Available online at www.sciencedirect.com
ScienceDirect
Trans. Nonferrous Met. Soc. China 35(2025) 1648−1661
Transactions of Nonferrous Metals Society of China
www.tnmsc.cn

Effect of binders on electrochemical properties of AgO cathode material for aqueous AgO−Al batteries

Xue-hua HE[1], Sheng-gui WANG[1,2], Yuan-kui WANG[2], Wan-li XU[3], Jue-min SONG[4,5], Zheng LI[4,5], Hai-tao ZHANG[1], Guang-zhou YANG[1], Xin-yi WANG[1], Qian ZHANG[1], Hong-xu LI[6], Kun YU[1,5]

1. School of Materials Science and Engineering, Central South University, Changsha 410083, China;
2. Kunming Branch of the 705 Research Institute, China State Shipbuilding Corporation Limited, Kunming 650032, China;
3. Institute of Systems Engineering, Academy of Military Sciences, Beijing 102300, China;
4. Hunan Hydro Dynamic New Materials Co., Ltd., Xiangtan 411101, China;
5. Hunan Center Special Metallurgy Novel Materials Research Institute, Changsha 410012, China;
6. Zijin Mining Group Co., Ltd., Xiamen 361008, China

Received 9 September 2023; accepted 4 April 2024

Abstract: To improve the slow kinetics and poor mechanical strength of aqueous silver peroxide−aluminum (AgO−Al) battery cathode materials, the effects of different binders including polytetrafluoroethylene (PTFE) and polyvinylpyrrolidone (PVP) on the AgO cathode material were investigated. The samples were characterized by scanning electron microscopy (SEM), transmission electron microscopy (TEM), cyclic voltammetry (CV), electrochemical impedance spectrum (EIS), and galvanostatic discharge. In contrast to the pure AgO and AgO−PTFE electrodes, the results demonstrated that the PVP effectively bound the electrode materials together. The prepared AgO−PVP as the cathode material of AgO−Al batteries could improve the battery capacity, exhibiting a high specific capacity (389.95 mA·h/g at 500 mA/cm^2), a high operating voltage (1.75 V at 500 mA/cm^2), a maximum energy density (665.65 W·h/kg), and a maximum power density (5236 W/kg). Furthermore, the electrochemical mechanism of the AgO−PVP cathode material was examined, revealing that the electrode exhibited rapid ion diffusion and effective interfacial ion/electron transport.

Key words: AgO; cathode material; high specific capacity; binder; aqueous AgO−Al batteries

1 Introduction

Aqueous silver peroxide−aluminum (AgO−Al) batteries have gained worldwide attention for their high energy density, long storage time, and fast discharge rate, making them ideal for military underwater applications, aerospace industries, and other fields [1−3]. The anode material is an aluminum (Al) alloy with low corrosion characteristics and is volumetrically superior to other non-lithium anode materials. The aluminum anodes have garnered considerable interest due to their abundant resources, high theoretical capacity, and safe chemistry [4−9]. The AgO cathode also plays a vital role in the electrochemical characteristics of batteries. A silver peroxide (AgO) battery was developed to increase the energy density of silver oxide. For a 2e reaction, the silver peroxide (AgO) has a theoretical capacity of up to 432 mA·h/g, which is approximately double the specific capacity (231 mA·h/g) of monovalent silver

Corresponding author: Kun YU, Tel: +86-13975808242, E-mail: yukun2010@csu.edu.cn
https://doi.org/10.1016/S1003-6326(25)66773-2

oxide (Ag_2O) [10]. Ag_2O can increase the battery's internal resistance during the discharge process due to its comparatively high electrical resistance.

Furthermore, AgO and its derivatives exhibit exceptional discharge rates, and often regarded as optimal materials for high-power electrodes [11]. The cathode limits the capacities of the AgO−Al battery to minimize the amount of expensive silver employed. In other words, the overall properties of AgO−Al battery are influenced mainly by the electrochemical behavior of the AgO cathode, rather than the aluminum anode.

Cathodes are typically composed of active material, binder, and conductive additive. Binders are an essential component that plays a critical role in maintaining the electrical connectivity of active material [12−15]. The binder plays a vital role in electrode formulation since it maintains the physical structure of the electrode. The electrode would disintegrate in the absence of a binder. An ideal binder must possess a high adhesion capacity to attach the electrode materials to the current collector, as well as the ability to establish a superior electric network between the active material and conductive material [16,17]. The AgO cathode exhibits poor mechanical strength leading to the detachment of the active material and subsequent decrease in electrode capacity during the discharge process.

An effective method for the electrochemical performance of AgO cathode is to enhance the mechanical stability of the electrode by adding a small amount of binder to the AgO electrode. Previous studies have extensively focused on binder materials, with polytetrafluoroethylene (PTFE) being the predominant binder utilized in the majority of AgO batteries [18−20]. Polyvinylidene fluoride (PVDF) [21], polyethylene oxide (PEO) [22] and polyacrylonitrile (PAN) have also been used as binders in the production of silver oxide cathodes for high-rate reserve batteries [23,24]. However, PVDF must be utilized in combination with the costly and hazardous reagent N-methyl-2-pyrrolidone (NMP). PAN shows instability in alkali and can be hydrolyzed to sodium polyacrylate in concentrated alkali above 80 °C, whereas PEO has weak thermal stability. Addressing this issue will not only determine the potential applications of additives but also significantly contribute to the advancement of AgO−Al batteries. PVP, a synthetic water-soluble polymer molecule, offers promising prospects due to its affordable cost, minimal toxicity, and superior biocompatibility.

This study introduces a simple and highly effective method for preparing AgO cathodes using various additives such as polytetrafluoroethylene (PTFE) and polyvinylpyrrolidone (PVP), and compares the electrochemical performance, morphology, and microstructure of the as-obtained AgO cathode materials during discharge. The results of electrochemical performance demonstrated that the AgO cathode with PVP binders had a high voltage plateau, enabling it to produce a much greater specific capacity at high discharge current densities compared to the pure AgO electrode or the electrode with PTFE binder. The reaction mechanism was investigated using a range of characterizations. The results confirmed that the electrode with a PVP binder exhibited the lowest charge transfer resistances and the highest ion diffusion rate. This improvement was attributed to the enhanced mechanical strength of the electrode, which facilitated better contact between the active substance and the electrolyte. This study offers environmentally friendly and high-performance AgO cathodes for aqueous AgO−Al batteries.

2 Experimental

2.1 Preparation of AgO cathode and characterization

All the chemical reagents were of analytical grade and used without any further purification. A high-purity AgO powder material was synthesized according to a previous report from our group [25]. To fabricate the AgO electrode, a binder solution (PVP blended with deionized water or PTFE blended with anhydrous ethanol) was combined with AgO active material to produce a homogenous slurry. This slurry was then poured onto a gold-plated current collector and dried at 60 °C for 5 h in a vacuum oven. The PVP has a polymerization degree of 17 and an approximate average relative molecular mass of 10000. Figure 1 depicts the chemical structures of the binders, polytetrafluoroethylene (PTFE) and polyvinylpyrrolidone (PVP), whereas Table 1 displays the composition of AgO cathode samples.

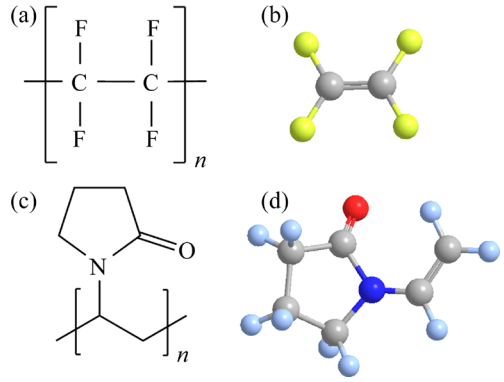

Fig. 1 Chemical structures (a, c) and monomer ball and stick models (b, d) of PTFE (a, b) and PVP (c, d)

Table 1 Compositions of slurries for AgO cathodes

Sample	Cathode slurry composition	Mass ratio of slurry
AgO−N	AgO	100
AgO−PTFE	AgO: PTFE: Super P	95:2.5:2.5
AgO−PVP	AgO: PVP: Super P	95:2.5:2.5

The morphology and microstructure of the prepared materials were assessed using field emission scanning electron microscopy (FE-SEM, TESCAN MIRA4, USA) and high-resolution transmission electron microscopy (HRTEM, JEM F200, JOEL). The crystal structures of all samples were recorded using a D/max 2500 X-ray powder diffractometer with a Cu K_α 40 kV/250 mA X-ray source. To analyze the chemical elements and valence state of the elements, X-ray photoelectron spectroscopic (XPS) analyses were performed using an ESCALAB 250 XI equipped with an Al monochromatic source and a charge neutralizer.

2.2 Electrochemical measurements

The electrochemical measurements were carried out using a standard three-electrode system, where the prepared AgO cathodes were used as the working electrodes, while a platinum sheet (4 cm^2) and a mercury/mercury oxide (Hg/HgO) electrode were used as the counter electrode and reference electrode, respectively. The active electrodes were developed by applying a layer of AgO slurry onto a gold-plated copper mesh current collector measuring 1 cm^2. For the experiments, a cathode with a mass of 246 mg was employed directly.

The galvanostatic discharge was measured using a Neware battery system (CT-4008-5V6A-S1) from China. CV and EIS were performed at room temperature using an electrochemical workstation (CHI660E, Chenhua, China). The potential during the CV measurements exhibited a range of 0.824−1.824 V (vs RHE). The EIS measurements were between 1×10^{-2} and 1×10^{5} Hz, with a 5 mV AC modulation amplitude. The results of the proposed equivalent circuit were evaluated by fitting the data using the Z-view electrochemical impedance spectroscopy analysis software (Scribner, Inc.).

The specific capacity (C), energy density (E), and power density (P) of the batteries were calculated using the following equations:

$$C=I\Delta t/m \tag{1}$$

$$E=I\int U\mathrm{d}t/m \tag{2}$$

$$P=E/\Delta t \tag{3}$$

where I, Δt, m, and U denote the discharge current, discharge time, mass load of active material, and discharge voltage, respectively.

The potentials observed against Hg/HgO were converted to the scale of the reversible hydrogen electrode (RHE) using the given equation ($\varphi_{RHE}=\varphi_{Hg/HgO}+0.098+0.059pH$).

3 Results and discussion

3.1 Material characteristics

Three different electrodes were prepared for electrochemical assessments, consisting of pure AgO, AgO combined with PTFE, and AgO combined with PVP. These electrodes were designated as AgO−N, AgO−PTFE, and AgO−PVP, respectively. Figure 2 depicts a schematic representation of the design and preparation process of the AgO−PVP cathode. Initially, a homogeneous mixture was prepared by combining AgO (5 g) and Super P carbon black (0.13 g). After that, the binder, PVP, which was dissolved in distilled water, was added to the mixed powder prepared in the first step, following the mass ratio specified in Table 1. The mixture was then stirred until it formed a homogenous slurry. After being evenly coated with the slurry, the collector was uniformly pressed to form a 1 mm-thick electrode. The electrode was then placed in a vacuum-drying oven and baked at 70 °C for 5 h. The AgO−PTFE electrode was fabricated using a similar procedure. For comparison, the AgO−N electrode, composed only of pure AgO,

was also made using the same method, but without the use of any binders.

Figures 3(a−c) demonstrate that the prepared electrodes have a porous surface structure that facilitates the transport and diffusion of ions. The AgO particles were loosely dispersed in the AgO−N electrode, the PTFE formed crosslinks with AgO particles in the AgO−PTFE electrode, and the PVP was tightly bonded to AgO particles in the AgO−PVP electrode. To evaluate the structure in

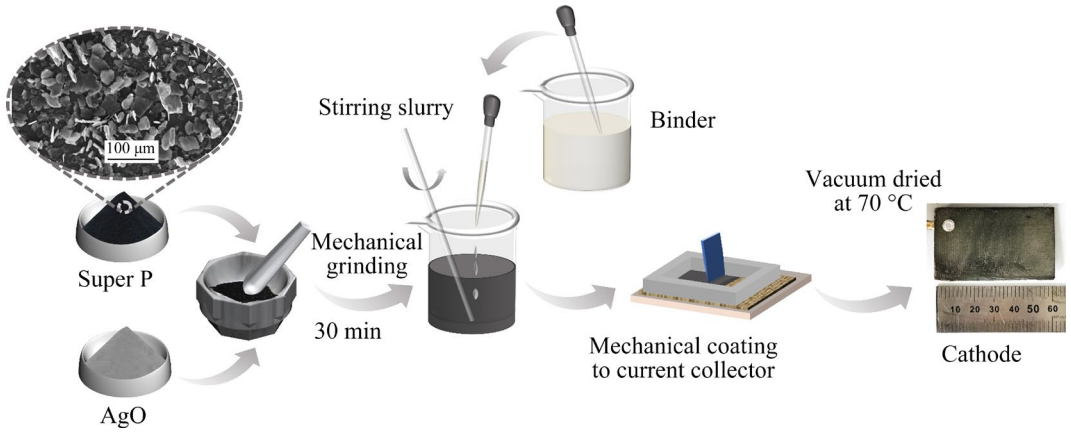

Fig. 2 Schematic illustration of AgO−PVP cathode fabrication process

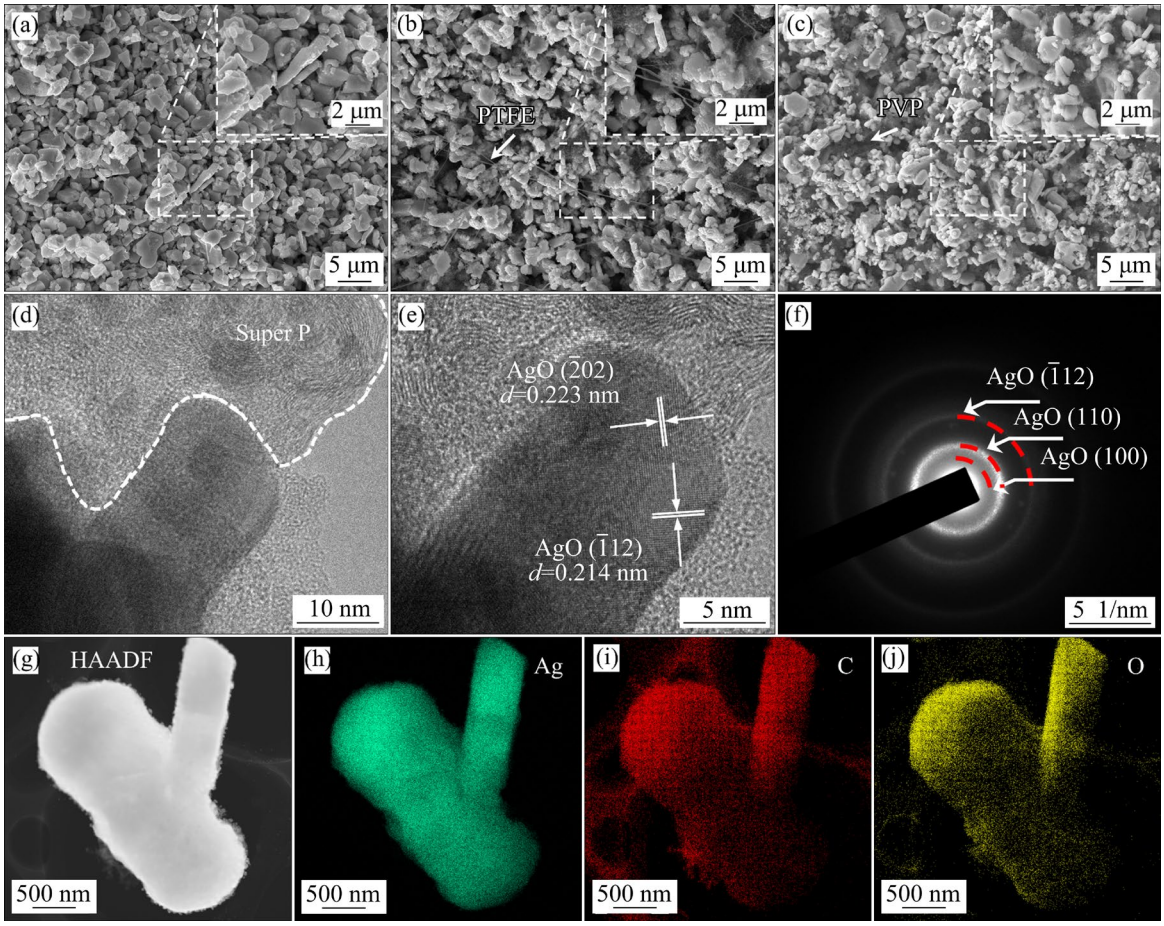

Fig. 3 FESEM images of AgO−N (a), AgO−PTFE (b) and AgO−PVP (c), TEM and HRTEM images of AgO−PVP electrode (d, e), selected area electron diffraction (SAED) pattern of AgO−PVP (f), high-angle annular dark-field scanning transmission electron microscopy (HAADF-STEM) image of AgO−PVP (g), and corresponding elemental mappings of Ag (h), C (i) and O (j)

detail, a high-resolution TEM (HRTEM) image of the AgO−PVP electrode was obtained, revealing clear lattice fringes and thus confirming the high degree of crystallinity. The existence of $(\bar{2}02)$ and $(\bar{1}12)$ crystallographic planes of AgO was confirmed based on the interplanar distances with spacings of 0.233 and 0.214 nm, respectively. The diffraction rings in the selected area electron diffraction (SAED) pattern (Fig. 3(f)) revealed the presence of (100), (110), and $(\bar{1}12)$ planes of AgO. The comparisons of high-angle annular dark-field scanning TEM (HAADF-STEM) and elemental mapping image of AgO−PVP (Figs. 3(g–j)) were utilized to establish the presence of the uniformly distributed elements Ag, C and O. The morphological characteristics of the AgO−PVP cathode exhibit highly desirable properties for achieving the ultra-efficient electrochemical performance in AgO−Al batteries.

3.2 Working mechanism of aqueous AgO−Al battery

The AgO−Al battery is an alkaline aqueous battery composed of silver peroxide (AgO) as the cathode material, aluminum (Al) as the anode, and an aqueous alkaline solution as the electrolyte. Al was selected as the anode due to its electrochemical characteristics and ease of fabrication. Sodium hydroxide serves as the electrolyte, facilitating the electrical conduction within the batteries through the participation of OH^- ions. The primary chemical reactions for reduction and oxidation at the cathode and anode are respectively given as [26]

Cathode:

$$3AgO(s)+3H_2O(l)+6e=3Ag(s)+6OH^-(aq) \quad (4)$$

Anode:

$$2Ag(s)+8OH^-(aq)=2AlO_2^-(aq)+4H_2O(l)+6e \quad (5)$$

The overall cell reaction is represented as

$$2Al(s)+3AgO(s)+2OH^-(aq)= 2AlO_2^-(aq)+H_2O(l)+3Ag(s) \quad (6)$$

The standard potential of this cell was calculated utilizing the standard free-energy data. Theoretical open circuit cell voltage varied between 2.695 and 2.952 V, depending on the oxidation state of silver. The maximum capacity of the AgO/Ag pair, as determined by a 2e reaction, was 432 mA·h/g. In addition, AgO and its derivatives exhibit exceptionally high discharge rates, making them often regard as optimal materials for high-power electrodes [11].

However, the operating potential of the batteries using Al as the anode material is generally lowered as a result of the parasitic corrosion of aluminum [27−29]. The reaction describing the corrosion of aluminum anode is given by

$$2Al(s)+2H_2O(l)+2OH^-(aq)=2AlO_2^-(aq)+3H_2(g) \quad (7)$$

The corrosion of aluminum at room temperature resulted in the production of an oxide layer, which subsequently led to an increase in the internal resistance of the battery. The optimal operating temperature for the battery was determined to be 82.5 °C, as it was observed that the evolution of H_2 gas was minimized at this temperature. The rate of H_2 evolution increased twofold for every 10 °C increase [30]. As a result, the battery selected a temperature of 80−85 °C for discharge.

3.3 Properties of assembled AgO−Al batteries

To assemble various AgO−Al batteries, AgO cathodes fabricated with different binders and Al alloy anodes were utilized. The electrolyte for these batteries was an aqueous solution comprising 4.5 mol/L NaOH and 20 g/L Na_2SnO_3. Na_2SnO_3 was added to inhibit the corrosion reaction of Al anode. The galvanostatic discharge profiles of AgO−Al batteries with cathodes composed of AgO and various binders at a current rate of 650 mA/cm^2 are illustrated in Fig. 4(a). The plateau of discharge voltage (1.65 V) for the AgO−Al battery with the AgO−PVP cathode was higher compared with the other two cathodes. As shown in Fig. 4(b), the open circuit voltages (OCVs) of AgO−Al batteries with different cathodes ranged from 2.4 to 2.5 V. As the discharge current density increased, there was a linear drop in the discharge voltage. The maximum output power density of the AgO−Al battery with AgO−PVP cathode was 1154.25 mW/cm^2, which was higher than that of the AgO−Al batteries with AgO−PTFE cathode (1085.94 mW/cm^2) and pure AgO cathode (999.00 mW/cm^2). This suggests that the shape of AgO−PVP, which includes a large specific surface area and porous structure, facilitates the efficient exposure of active sites. The rate performance of AgO−Al batteries with AgO−PVP electrodes was evaluated by measuring

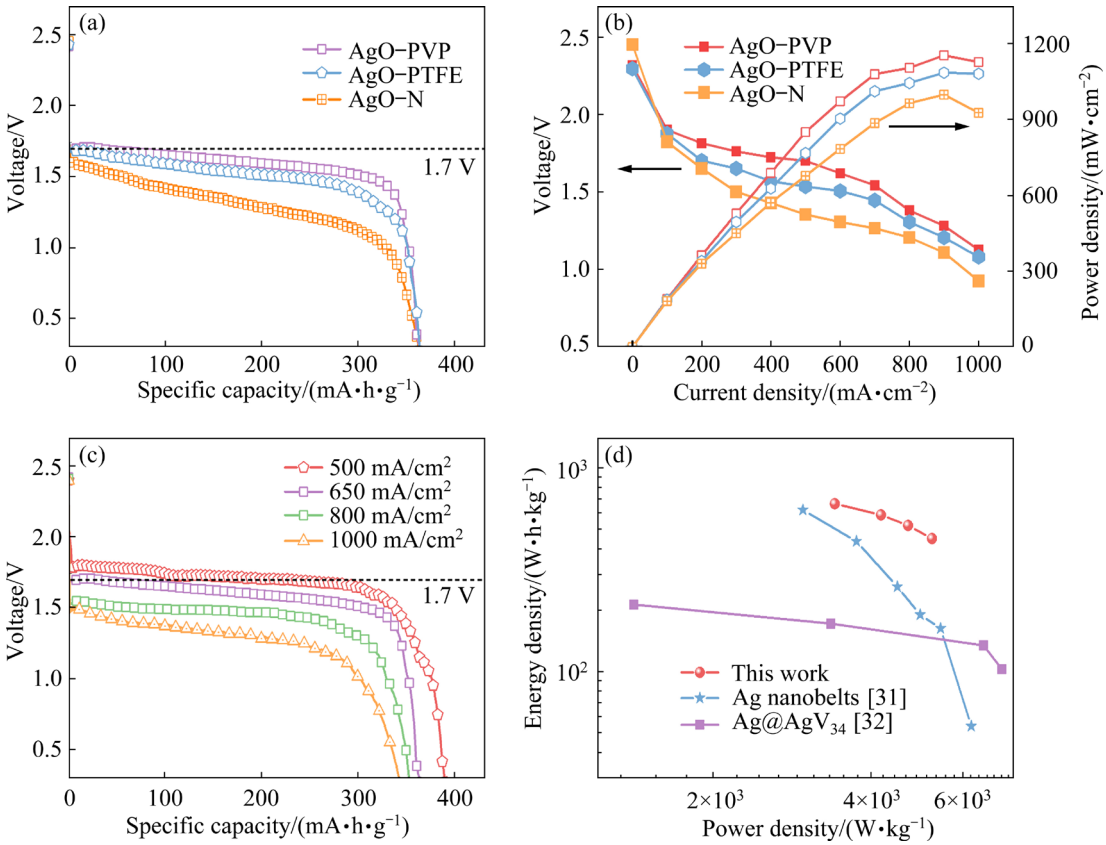

Fig. 4 Electrochemical properties of AgO−Al batteries: (a) Galvanostatic discharge curves of AgO−Al batteries fabricated using different binders under discharge current density of 650 mA/cm^2; (b) Discharge profiles and corresponding power densities for cathode with different binders; (c) Comparison of specific capacity of AgO−Al battery with AgO−PVP cathode under different discharge current densities; (d) Ragone plot of comparing performance for AgO−Al battery with AgO−PVP cathode to reported literature values

the galvanostatic discharge at different current densities. Figure 4(c) displays the galvanostatic discharge curves at various current densities (500, 650, 800, and 1000 mA/cm^2) in the voltage range of 2.5−0.3 V. The AgO−Al battery experienced a decrease in capacity as the current density increased, mostly because the polarization effect became more pronounced during discharge [31]. The AgO−Al battery with AgO−PVP cathode exhibited an operating voltage plateau of 1.75 V and a corresponding capacity of 389.95 mA·h/g at a current density of 500 mA/cm^2. At the maximum current density of 1000 mA/cm^2, the values were greater than 1.3 V and 343.22 mA·h/g, respectively. In addition, the aqueous AgO−Al battery with AgO−PVP cathode achieved a maximum energy density of 665.65 W·h/kg and a maximum power density of 5236 W/kg (based on the mass of AgO), as demonstrated by the Ragone plot in Fig. 4(d). These values surpass those reported in existing literature. Furthermore, the specific capacity of the battery with AgO−PVP cathode was either comparable to or higher than that of previously reported silver-based batteries (Table 2), including

Table 2 Comparison of cathodes used in silver-based batteries

Cathode material	Current density/(mA·cm^{-2})	Specific capacity/(mA·h·g^{-1})	Ref.
AgO/CMC	600	344	[18]
AgO/PAN	600	313	[23]
AgO/PVDF	600	321	[23]
AgO/CMC&SBR	1000	285	[25]
Ag nanobelts	10	260.7	[31]
Ag@AgV$_{34}$	12*	176	[32]
AgO−PVP	500	389.95	This work
AgO−PVP	1000	343.22	This work

* A/g

AgO/CMC (344 mA·h/g at 600 mA/cm^2) [18], AgO/PAN (313 mA·h/g at 600 mA/cm^2) [23], AgO/PVDF (321 mA·h/g at 600 mA/cm^2) [23], AgO/CMC&SBR (285 mA·h/g at 1000 mA/cm^2) [25], Ag nanobelts (260.7 mA·h/g at 10 mA/cm^2) [31], and Ag@AgV_{34} (176 mA·h/g at 12 A/g) [32]. This confirms that PVP, as a binder, is superior in improving the discharge performance of the AgO cathode in the aqueous AgO−Al battery.

3.4 Electrochemical reaction kinetics

A cyclic voltammetric analysis was conducted to investigate the energy storage mechanism of the AgO−PVP electrode. The CV curve at a scanning rate of 1.0 mV/s exhibited two pairs of redox peaks, as illustrated in Fig. 5(a). AgO/Ag_2O and Ag_2O/Ag are two redox couples for the AgO−PVP electrode [33]. Two distinct oxidation peaks were identified during the process of converting Ag to Ag_2O and Ag_2O to AgO. These peaks occurred at 1.38 V and 1.59 V (vs RHE), respectively. The reduction peaks for the conversion of AgO to Ag_2O and Ag_2O to Ag were observed at 1.33 and 1.02 V (vs RHE), respectively. These reactions are divided into two steps, as illustrated in Eqs. (8) and (9) [34−41]:

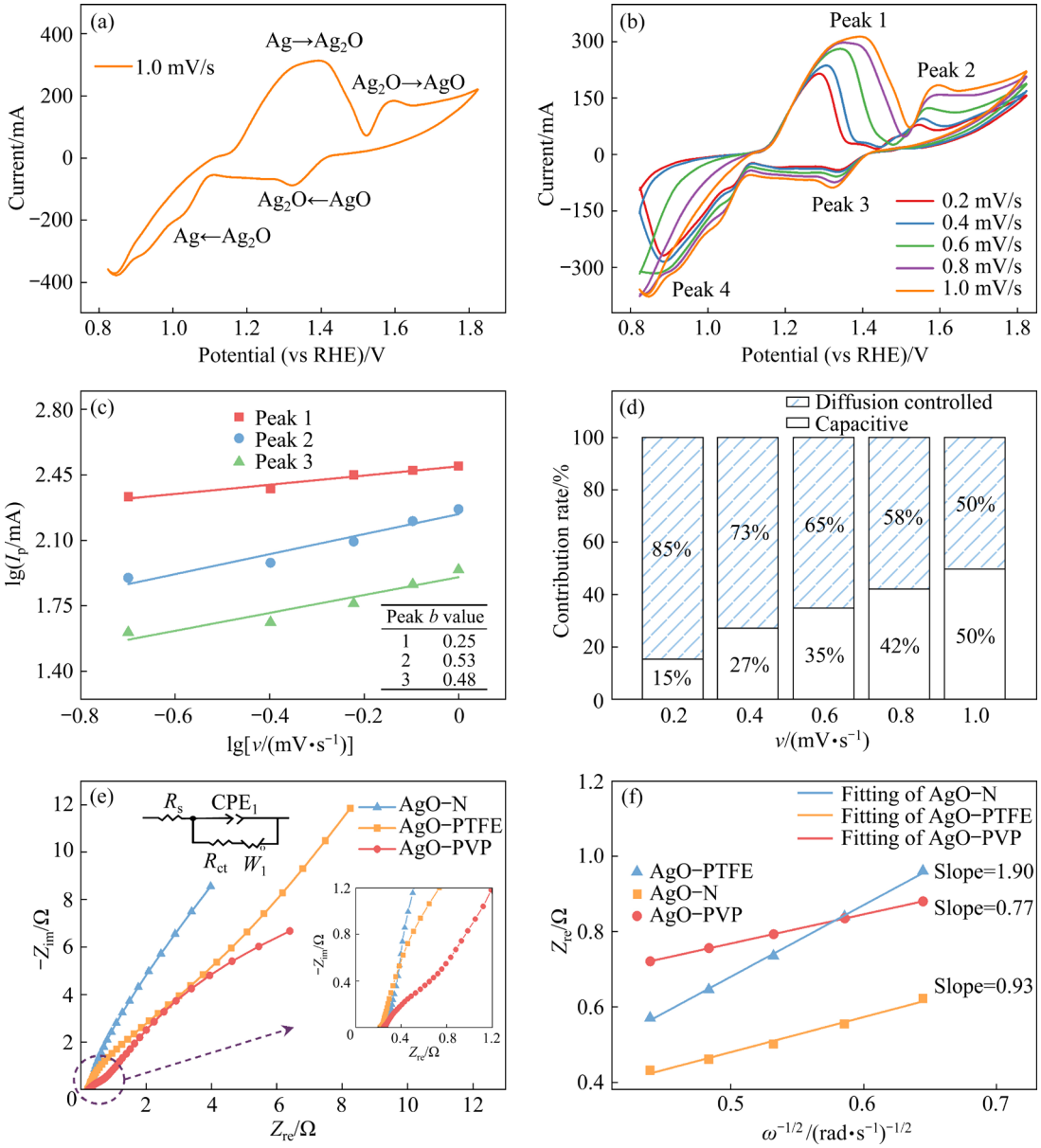

Fig. 5 (a) Cyclic voltammogram of AgO−PVP electrode at scanning rate of 1.0 mV/s; (b) Cyclic voltammogram of AgO−PVP electrode at different scanning rates; (c) lg I_p versus lg v plots of three peaks in CV curves; (d) Capacitive and diffusion contribution rates of CV curves; (e) Nyquist plots for AgO−N, AgO−PTFE and AgO−PVP (Inset: enlarged plot in high-frequency range); (f) Relationship between real part of impedance and low angular frequency (ω)

Step I: $2AgO+H_2O+2e=Ag_2O+2OH^-$ (8)

Step II: $Ag_2O+H_2O+2e=2Ag+2OH^-$ (9)

Following that, a series of CV experiments were conducted at different scanning rates (0.2 to 1.0 mV/s) to investigate the electrochemical storage kinetics of the AgO−PVP cathode (Fig. 5(b)). The voltages of Peaks 1 and 2 increased gradually with the scanning rate, whereas the voltage of Peaks 3 and 4 decreased. The variation in voltage and gradual removal of reduction Peak 4 at higher scanning rates can be attributed to the electrode polarization. The relationship between the peak current (I, mA) and the scanning rate (v, mV/s) is described by the equation of $I=av^b$, where a and b are adjustable constants, and the b values are obtained from the fit. In general, the value of b falls in the range of 0.5−1. A value of b=0.5 implies a diffusion-controlled electrochemical process, whereas a value of b=1 indicates a capacitive-limited process [42]. From the fitting plots of peaks 1, 2 and 3 in Fig. 5(c), it can be observed that the values of b for each peak were 0.25, 0.53 and 0.48, respectively. These values indicate that the AgO−PVP electrode undergoes a diffusion-controlled electrochemical reaction. Furthermore, according to the equation of $I=k_1v+k_2v^{1/2}$, the terms k_1v and $k_2v^{1/2}$ represent the capacitive-limited and diffusion-controlled components, respectively [43]. Figure 5(d) shows that at the scanning rates of 0.2, 0.4, 0.6, 0.8 and 1.0 mV/s, the respective diffusion contributions were 85%, 73%, 65%, 58% and 50% respectively. This further confirms that the diffusion process plays a significant part in the overall capacity. The high diffusion contribution rate is advantageous due to the porous structure, which has a large specific surface area and numerous reaction sites, which facilitates rapid ions diffusion.

An electrochemical impedance spectroscopy (EIS) analysis was conducted using an open circuit voltage (OCV) to investigate the electrochemical kinetics and resistance of the AgO cathodes with various binders. Figure 5(e) presents Nyquist plots of electrodes AgO−N, AgO−PTFE, and AgO−PVP. An inset of Fig. 5(e) illustrates the relevant fitting equivalent circuit. All the curves showed a similar shape, indicating a slash in the low-frequency region and a semicircle in the high and middle-frequency regions. The semicircle and slash were associated with the charge transfer resistance (R_{ct}) and diffusion migration resistance (R_s), respectively. The diameter of the semicircle in the high-frequency range was shown to be directly connected to the charge-transfer resistance. The R_{ct} values of AgO−N, AgO−PTFE and AgO−PVP measured by EIS analysis were 5.09, 3.93 and 0.84 Ω, respectively. The AgO−PVP electrode had the lowest charge transfer resistance, indicating its exceptional electrochemical performance.

To further validate these findings, the diffusion coefficient for OH^- ions (D_{OH^-}) was calculated using Eqs. (10) and (11) to assess its capacity for diffusion within the material.

$$Z_{re}=R_s+R_{ct}+\sigma\omega^{-1/2} \tag{10}$$

$$D_{OH^-}=\frac{R^2T^2}{2A^2n^2F^4C^2\sigma^2} \tag{11}$$

In Eq. (10), σ represents the Warburg factor, which may be determined from the linear fitting between $\omega^{-1/2}$ and Z_{re} (Warburg impedance) at low frequency, as shown in Fig. 5(f). The fitted values of b for the AgO−N, AgO−PTFE and AgO−PVP electrodes were 1.90, 0.93 and 0.77, respectively. The diffusion coefficient for OH^- ions in the three cathodes was determined using Eq. (11), where R, T, A, n, F and C denote the molar gas constant, temperature, electrode area, electron transfer number of OH^- ions, Faraday constant, and concentration of OH^- electrolyte, respectively. By analyzing the σ values obtained from Fig. 5(f), it was determined that the OH^- diffusion coefficient of AgO−PVP is significantly greater than that of AgO−PTFE and AgO−N. The AgO−PVP electrode had the highest rate of OH^- ion diffusion, providing further evidence of its low diffusion resistance.

According to the CV and EIS analysis, it can be concluded that the AgO−PVP structure provides the electrode with rapid ion diffusion and effective interfacial ion/electron transport capabilities.

3.5 Energy storage mechanism

To gain a deep understanding of the process of energy storage, various characterizations were conducted to highlight the operational mechanism of the AgO−PVP electrode during the discharging phase. Figure 6(a) depicts the discharge process of the AgO−PVP electrode at a current density of 250 mA/cm^2. The mechanism of the discharge process was investigated by examining various discharge states, which are represented by Points A

to *I* on the curve. To obtain a more comprehensive understanding of the energy storage mechanism of AgO−PVP cathode materials, numerous ex-situ XRD experiments were conducted to analyze the structural evolution of the material across different discharge states (Figs. 6(b, c)). At a charge of 1.02 V (*B*), the distinctive peaks ($\bar{1}11$), (002), (111) and ($\bar{2}02$) of AgO (JCPDS# 43-1038) were still visible at angles of 32.2°, 34.2°, 37.2° and 39.4°, respectively. The analysis also demonstrated the gradual evolution of the distinctive peak (111) of Ag_2O (JCPDS# 41−1104) at an angle of 32.8°, indicating the intercalation of OH^- ions into the cathode interlayer. As the voltage was discharged further to 0.92 V (*C*), the signal from AgO nearly disappeared and the intensity of the distinct peak (111) at 32.8° of Ag_2O decreased. Moreover, the formation of the final product silver (JCPDS# 04-6436) was observed upon additional discharge of voltage to 0.72 V (*D*). The discharge state of *E* and *I* was only observed in the case of silver, followed by a relatively rapid drop in discharge voltage.

The chemical configurations of the AgO−PVP cathode were examined using ex-situ XPS spectroscopy in the pristine, discharged condition *B*, and completely discharged state. Figure 6(d) displays the complete XPS spectrum, revealing no noticeable change in shape. The high-resolution XPS spectrum for Ag 3d displayed two distinct peaks (Fig. 6(e)) at energy levels of 367.88 and 373.58 eV. These peaks correspond to the Ag $3d_{5/2}$ and Ag $3d_{3/2}$ states, respectively. The analysis of the Ag $3d_{5/2}$ spectrum revealed the existence of two distinct peaks at 366.98 and 368.12 eV, which corresponded to the Ag^+ and Ag^{3+} states, respectively. Furthermore, the deconvoluted Ag $3d_{3/2}$ spectrum displayed two distinct peaks at 372.78 and 374.18 eV, which can be attributed to Ag^+ and Ag^{3+} ions, respectively. The presence of Ag^{3+} species was observed exclusively in the *A* and *B* states (Fig. 6(e)). The Ag $3d_{3/2}$ peak shifted towards higher

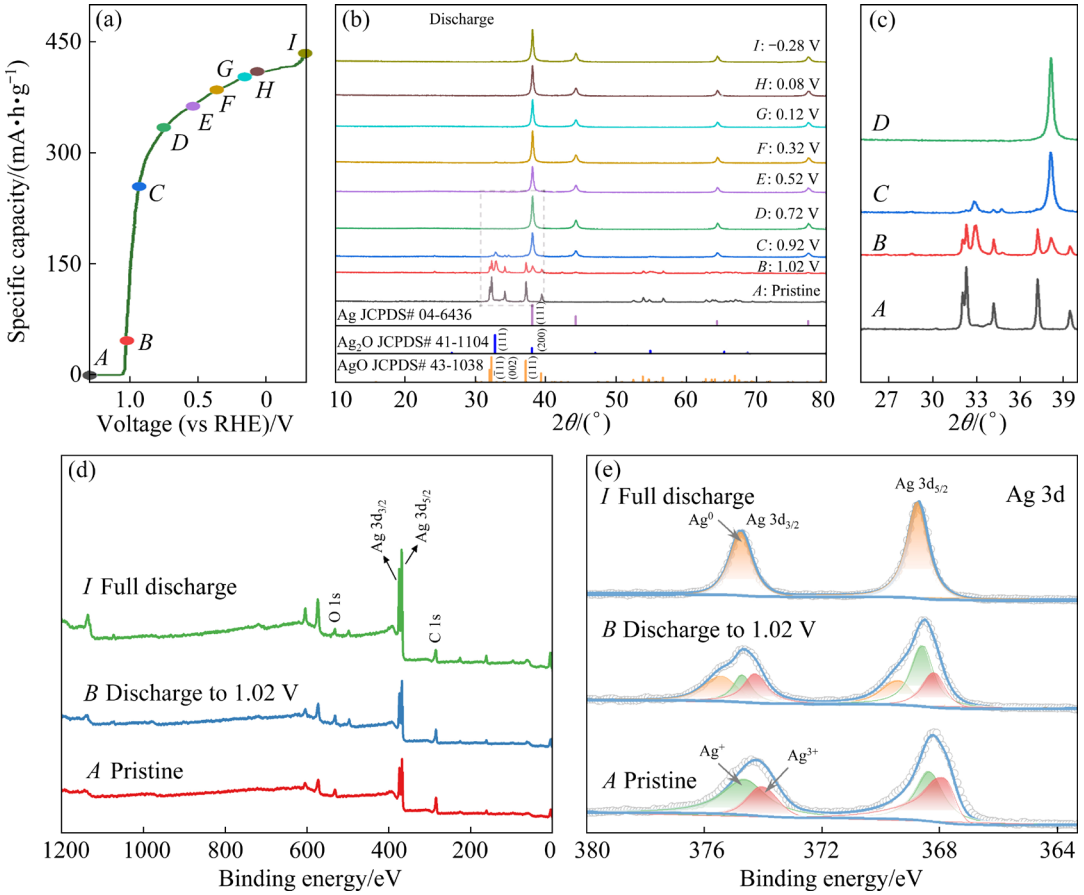

Fig. 6 Mechanistic study of discharge storage: (a) Discharge curves of AgO−PVP electrode at current density of 250 mA/cm^2; (b) Evolution of ex-situ XRD patterns of AgO−PVP cathode during discharge process; (c) Selected ex-situ XRD patterns from (b) at scanning angles of 25°−40°; (d) Ex-situ XPS full survey spectra of AgO cathode in different discharge states; (e) Ex-situ high-resolution XPS spectra of Ag 3d for AgO cathode in different discharge states

binding energy and disappeared during full discharge, suggesting an increase in Ag^+ species at approximately 1.02 V due to the incorporation of OH^- ions into the cathode during discharge. This led to further reduction of Ag^{3+} species to Ag^+ and ultimately to Ag, aligning with the findings of ex-situ XRD.

Figure 7 depicts SEM images of the AgO−PVP electrode at several discharge voltages. Compared to the morphology of the original electrode shown in Fig. 3(c), fine nanoparticles were found to be attached to the flaky AgO particles when discharged to 1.02 V (Fig. 7(a)), and the flaky particles gradually disappeared when discharged to 0.92 and 0.12 V (Figs. 7(b) and (c)), leaving only fine nanoscale particles. The porosity of the electrode surface increased even more when it was fully discharged (Fig. 7(d)), as the binder was strongly bound with the nanoparticles. During discharge, the active component AgO underwent reduction to Ag_2O, which ultimately reduced to Ag. During the reduction process, the volume of the surface particles decreased due to the high density of Ag, resulting in an increase in porosity at the end of discharge.

The TEM image of the fully discharged state of the AgO−PVP electrode is shown in Fig. 8. The surface phase of the discharge result is evident as flake nanoparticles, as depicted in Figs. 8(a) and (c). The selected area electron diffraction (SAED) pattern (Fig. 8(b)) reveals distinct diffraction rings that indicate the presence of phases corresponding to the (111), (002), (022), and (222) planes of Ag. The HRTEM image of the electrode in the fully discharged state, as depicted in Fig. 8(d), reveals lattice dimensions of 0.207 and 0.227 nm. These dimensions correspond to the (200) and (111) crystal lattice planes of the cubic Ag phase, respectively. A silver layer of the discharged product promotes the participation of unreacted AgO active material in the electrochemical reaction due to its higher conductivity. The exceptional performance of the AgO−Al battery can be attributed to the remarkable conductivity of AgO and its reduction product of Ag.

The aforementioned ex-situ measurements and analyses provide insight into the superior electrochemical performance of AgO−PVP electrodes. The porous structure of the electrode surface facilitates the diffusion and migration of ions. Due to the semiconducting properties of AgO and the insulating properties of the PVP binder, both AgO and its resulting silver product serve as conductors to establish electrical connections between the

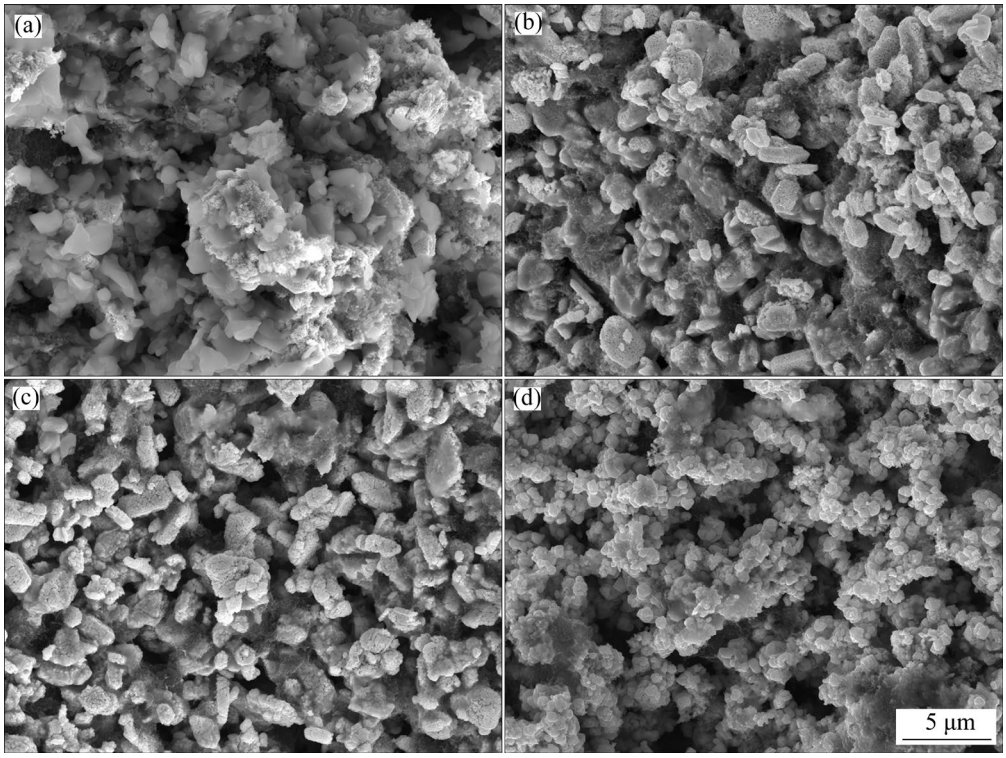

Fig. 7 SEM images of AgO−PVP electrode at different discharge voltages: (a) 1.02 V; (b) 0.92 V; (c) 0.12 V; (d) Full discharge

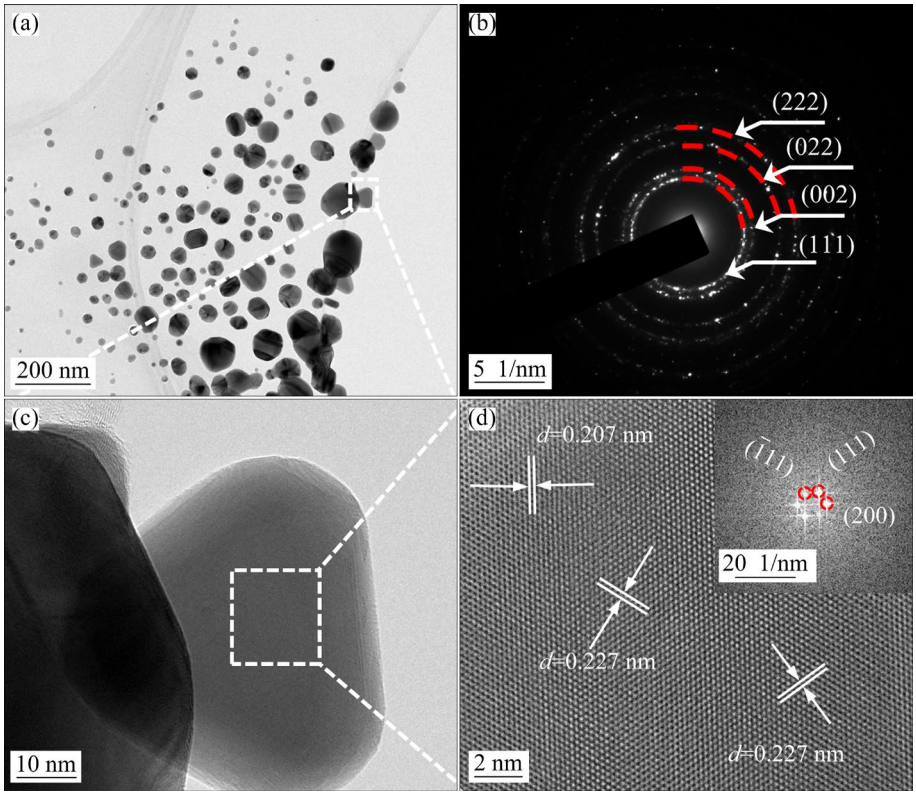

Fig. 8 Characterization results of AgO−PVP cathode at fully discharged state: (a, c) TEM images; (b) SAED pattern; (d) HRTEM image and corresponding FFT pattern (inset)

cathode particles and the cathode pellet. In conclusion, the AgO−Al batteries made using the AgO−PVP electrode show great potential for use in energy storage systems.

4 Conclusions

(1) A systematic investigation of aqueous AgO−Al batteries using several binders (none, PVP, and PTFE) showed that the cathodes fabricated with PVP binder exhibited superior electrochemical performance.

(2) The assembled aqueous AgO−Al battery employing AgO−PVP cathode achieved a maximum energy density of 665.65 W·h/kg, maximum power density of 5236 W/kg, and exhibited excellent rate capability (389.95 and 343.22 mA·h/g at 500 and 1000 mA/cm^2, respectively). The mechanistic studies reveal that the rapid diffusion of OH^- ions and electron transport play a crucial role in determining the overall capacity of the AgO−PVP cathode material.

(3) According to the findings of CV and EIS analysis, it can be concluded that the AgO−PVP structure imparts rapid ion diffusion and effective interfacial ion/electron transport capabilities to the electrode. The study demonstrates the promising application prospects of the AgO electrode when combined with PVP as a binder. It also presents a new strategy for investigating and developing high-performance aqueous AgO−Al batteries.

CRediT authorship contribution statement

Xue-hua HE: Investigation, Experiment, Drawing, Writing – Original draft, Writing − Review & editing; **Sheng-gui WANG:** Investigation, Experiment; **Yuan-kui WANG:** Formal analysis, Funding acquisition; **Wan-li XU:** Data curation, Supervision, Project administration; **Jue-min SONG:** Data curation, Drawing, Writing – Review & editing; **Zheng LI:** Writing – Review & editing, Investigation; **Hai-tao ZHANG** and **Guang-zhou YANG:** Validation, Investigation; **Xin-yi WANG:** Experiment, Data curation, Writing – Review & editing; **Qian ZHANG:** Writing – Review & editing; **Hong-xu LI:** Conceptualization, Data curation; **Kun YU:** Funding acquisition, Conceptualization, Methodology.

Declaration of competing interest

The authors declare that they have no known competing financial interests or personal relationships

that could have appeared to influence the work reported in this paper.

Acknowledgments

This work was financially supported by the Fundamental Research Funds for the Central Universities of Central South University, China (No. 2022XQLH046), the Technical Area Fund of Foundation Strengthening, China (No. 2022-JCJQ-ZD-174-00-20), National Defense Basic Scientific Research Projects, China, and Central South University−Zijin Mining Technical Cooperation Development Project, China.

References

[1] GONZALEZ-GUERRERO M J, GOMEZ F A. Miniaturized Al/AgO coin shape and self-powered battery featuring painted paper electrodes for portable applications [J]. Sensors and Actuators B: Chemical, 2018, 273: 101−107. https://doi.org/10.1016/j.snb.2018.06.016.

[2] NAHIDI S, BEHROOZIZADE E. The effect of anode and cathode separators in Al−AgO battery on the hydrodynamic of electrolyte [J]. Fluid Mechanics & Aerodynamics Journal, 2022, 10(2): 125−140.

[3] CHEN Jin-mao, XU Wan-li, WANG Xu-dong, YANG Sha-sha, XIONG Chun-hua. Progress and applications of seawater-activated batteries [J]. Sustainability, 2023, 15(2): 1635. https://doi.org/10.3390/su15021635.

[4] WU Zi-bin, ZHANG Hai-tao, ZOU Jing, SHEN Xiao-dong, QIN Ke, BAN Chun-yan, CUI Jian-zhong, NAGAUMI H. Enhancement of the discharge performance of Al−0.5Mg−0.1Sn−0.05Ga (wt.%) anode for Al−air battery by directional solidification technique and subsequent rolling process [J]. Journal of Alloys and Compounds, 2020, 827: 154272. https://doi.org/10.1016/j.jallcom.2020.154272.

[5] WU Zi-bin, ZHANG Hai-tao, ZHENG Yu-qian, ZOU Jing, YANG Dong-hui, GUO Cheng, QIN Ke, BAN Chun-yan, CUI Jian-zhong, NAGAUMI H. Electrochemical behaviors and discharge properties of Al−Mg−Sn−Ca alloys as anodes for Al-air batteries [J]. Journal of Power Sources, 2021, 493: 229724. https://doi.org/10.1016/j.jpowsour.2021.229724.

[6] AFSHARI M, ABBASI R, SOVIZI M R. Evaluation of nanometer-sized zirconium oxide incorporated Al−Mg−Ga−Sn alloy as anode for alkaline aluminum batteries [J]. Transactions of Nonferrous Metals Society of China, 2020, 30(1): 90−98. https://doi.org/10.1016/s1003-6326(19)65182-4.

[7] YANG Hui-cong, LI Hu-cheng, LI Juan, SUN Zhen-hua, HE Kuang, CHENG Hui-ming, LI Feng. The rechargeable aluminum battery: Opportunities and challenges [J]. Angewandte Chemie International Edition, 2019, 58(35): 11978−11996. https://doi.org/10.1002/anie.201814031.

[8] GAO Jian-xin, LI Yang, YAN Zhao, LIU Qian-feng, GAO Yan-li, CHEN Chang-ke, MA Bing, SONG Yu-jiang, WANG Er-dong. Effects of solid-solute magnesium and stannate ion on the electrochemical characteristics of a high-performance aluminum anode/electrolyte system [J]. Journal of Power Sources, 2019, 412: 63−70. https://doi.org/10.1016/j.jpowsour.2018.11.019.

[9] ZHUANG Ze-hang, FENG Yan, PENG Chao-qun, YANG Liu-zhong, WANG Meng. Effect of Ga on microstructure and electrochemical performance of Al−0.4Mg−0.05Sn−0.03Hg alloy as anode for Al−air batteries [J]. Transactions of Nonferrous Metals Society of China, 2021, 31(9): 2558−2569. https://doi.org/10.1016/s1003-6326(21)65675-3.

[10] LI Hui-qiao, WANG Yong-gang, HE Ping, ZHOU Hao-shen. A novel rechargeable Li−AgO battery with hybrid electrolytes [J]. Chemical Communications, 2010, 46(12): 2055−2057. https://doi.org/10.1039/b923706b.

[11] ZHOU Hao-shen, WANG Yong-gang, LI Hui-qiao, HE Ping. The development of a new type of rechargeable batteries based on hybrid electrolytes [J]. ChemSusChem, 2010, 3(9): 1009−1019. https://doi.org/10.1002/cssc.201000123.

[12] WANG Hui, ZHANG Guang-zhao, CHEN Yu-kun, ZHENG Pei-tao, YI Huan, DENG Yong-hong, YANG Yu, WANG Chao-yang. Reversible cross-linked phosphorylate binder for recyclable lithium-sulfur batteries [J]. Chemical Engineering Journal, 2023, 452: 139128. https://doi.org/10.1016/j.cej.2022.139128.

[13] CHANG H J, PODRÍGUEZ-PÉREZ I A, FAYETTE M, CANFIELD N L, PAN H L, CHOI D, LI Xiao-lin, REED D. Effects of water-based binders on electrochemical performance of manganese dioxide cathode in mild aqueous zinc batteries [J]. Carbon Energy, 2021, 3(3): 473−481. https://doi.org/10.1002/cey2.84.

[14] LIANG Jian-neng, CHEN Da-chang, ADAIR K, SUN Qian, HOLMES N G, ZHAO Yang, SUN Yi-peng, LUO Jing, LI Ru-ying, ZHANG Li, ZHAO Shang-qian, LU Shi-gang, HUANG Huan, ZHANG Xiao-xing, SINGH C V, SUN Xue-liang. Insight into prolonged cycling life of 4 V all-solid-state polymer batteries by a high-voltage stable binder [J]. Advanced Energy Materials, 2021, 11(1): 2002455. https://doi.org/10.1002/aenm.202002455.

[15] WANG Rui, FENG Li-li, YANG Wen-rong, ZHANG Yin-yin, ZHANG Yan-li, BAI Wei, LIU Bo, ZHANG Wei, CHUAN Yong-ming, ZHENG Zi-guang, GUAN Hong-jin. Effect of different binders on the electrochemical performance of metal oxide anode for lithium-ion batteries [J]. Nanoscale Research Letters, 2017, 12: 575. https://doi.org/10.1186/s11671-017-2348-6.

[16] LI Chen, SUN Qi-fang, ZHANG Qing, XU Chao-ran, WANG Su, MA Yue, SHI Xi-xi, ZHANG Hong-zhou, SONG Da-wei, ZHANG Lian-qi. Multifunctional binder capable of promoting the reaction dynamics of wide temperature operable lithium-sulfur battery [J]. Chemical Engineering Journal, 2023, 455: 140706. https://doi.org/10.1016/j.cej.2022.140706.

[17] JANG W, KIM S, KANG Y M, YIM T, KIM T H. A high-performance self-healing polymer binder for Si anodes based on dynamic carbon radicals in cross-linked poly(acrylic acid) [J]. Chemical Engineering Journal, 2023, 469: 143949. https://doi.org/10.1016/j.cej.2023.143949.

[18] NAJAFI M, ABEDINI A. The effect of dimensional ratio and proportion of micron-nanoparticles on discharge performance of silver (II) oxide cathode [J]. Ionics, 2019,

25(7): 3269−3276. https://doi.org/10.1007/s11581-019-02880-2.

[19] TAKEDA K, HATTORI T. Optimization of the amount of additives to AgO cathodes on high-drain pulse performance of Zn/AgO cells [J]. Journal of the Electrochemical Society, 2001, 148(1): A44. https://doi.org/10.1149/1.1339028.

[20] OZGIT D, HIRALAL P, AMARATUNGA G A J. Improving performance and cyclability of zinc–silver oxide batteries by using graphene as a two dimensional conductive additive [J]. ACS Applied Materials & Interfaces, 2014, 6(23): 20752−20757. https://doi.org/10.1021/am504932j.

[21] VILKHU R, THIO W J, GHATAK P D, SEN C K, CO A C, KIOURTI A. Power generation for wearable electronics: Designing electrochemical storage on fabrics [J]. IEEE Access, 2018, 6: 28945−28950. https://doi.org/10.1109/ACCESS.2018.2839078.

[22] KUMAR R, JOHNSON K M, WILLIAMS N X, SUBRAMANIAN V. Scaling printable Zn−Ag_2O batteries for integrated electronics [J]. Advanced Energy Materials, 2019, 9(13): 1803645. https://doi.org/10.1002/aenm.

[23] NAJAFI M, ABEDINI A. The critical role of polymeric binders on AgO cathodes in high rate batteries [J]. Thin Solid Films, 2021, 721: 138532. https://doi.org/10.1016/j.tsf.2021.138532.

[24] KOTA A, KUM L W, VALLURUPALLI K, GOGIA A, NEIDHARD-DOLL A T, CHODAVARAPU V P. Highly flexible stencil printed alkaline Ag_2O−Zn battery for wearable electronics [J]. Batteries, 2022, 8(7): 74. https://doi.org/10.3390/batteries8070074.

[25] HE Xue-hua, LI Zheng, WANG Yuan-kui, XU Wan-li, ZHANG Qian, WANG Xin-yi, LIU Hui, YANG Guang-zhou, ZHANG Hai-tao, SONG Jue-min, WANG Sheng-gui, LU Chang-bo, YU Kun. A high-purity AgO cathode active material for high-performance aqueous AgO−Al batteries [J]. Journal of Power Sources, 2022, 551: 232151. https://doi.org/10.1016/j.jpowsour.2022.232151.

[26] MEDEIROS M G, ZOSKI C G. Investigation of a sodium hypochlorite catholyte for an aluminum aqueous battery system [J]. The Journal of Physical Chemistry B, 1998, 102(49): 9908−9914. https://doi.org/10.1021/jp982825p.

[27] ASFIA M P, POURFARZAD H, KASHANI H, OLIA M H, BADRNEZHAD R. Study of uniform and localized corrosion behaviour of aluminum alloy 1050 as Al/AgO battery anode in aerated NaCl in the presence of an organosulfur inhibitor [J]. Journal of the Electrochemical Society, 2020, 167(14): 140527. https://doi.org/10.1149/1945-7111/abc438.

[28] MOGHANNI-BAVIL-OLYAEI H, ARJOMANDI J. Enhanced electrochemical performance of Al−0.9Mg−1Zn−0.1Mn−0.05Bi−0.02In fabricated from commercially pure aluminum for use as the anode of alkaline batteries [J]. RSC Advances, 2016, 6(33): 28055−28062. https://doi.org/10.1039/C6RA02113A.

[29] SRINIVAS M, ADAPAKA S K, NEELAKANTAN L. Solubility effects of Sn and Ga on the microstructure and corrosion behavior of Al−Mg−Sn−Ga alloy anodes [J]. Journal of Alloys and Compounds, 2016, 683: 647−653. https://doi.org/10.1016/j.jallcom.2016.05.090.

[30] GOTTFREDSON R K. Advanced concepts for lightweight torpedo propulsion [R]. San Diego, CA (USA): Naval Ocean Systems Center, 1979.

[31] YANG Lu-fa, HE Shuai, SHANG Zong-yi, ZOU Jie, YANG Yao-yue, ZHAO Zhi-gang, XIAO Dan, ZHOU Cai-xia. High-performance aqueous rechargeable Zn−Ag and Zn−Ag/air hybrid batteries based on Ag nanobelts as highly stable bifunctional electrode [J]. Applied Surface Science, 2023, 608: 155236. https://doi.org/10.1016/j.apsusc.2022.155236.

[32] YANG Kai, YING Yu-xuan, CUI Lu-lu, SUN Jian-chao, LUO Hao, HU Yuan-yuan, ZHAO Jun-wei. Stable aqueous Zn−Ag and Zn−polyoxometalate hybrid battery driven by successive Ag+ cation and polyoxoanion redox reactions [J]. Energy Storage Materials, 2021, 34: 203−210. https://doi.org/10.1016/j.ensm.2020.09.011.

[33] HONG Hong, JIANG Li-hong, TU Hua-ting, HU Ji-yong, MOON K S, YAN Xiong, WONG C P. Rational design and evaluation of UV curable nano-silver ink applied in highly conductive textile-based electrodes and flexible silver-zinc batteries [J]. Journal of Materials Science & Technology, 2022, 101: 294−307. https://doi.org/10.1016/j.jmst.2021.04.061.

[34] CHANG C C, LEE Y C, LIAO H J, KAO Y T, AN J Y, WANG D Y. Flexible hybrid Zn−Ag air battery with long cycle life [J]. ACS Sustainable Chemistry & Engineering, 2019, 7(2): 2860−2866. https://doi.org/10.1021/acssuschemeng.8b06328.

[35] SHANG Wen-xu, YU Wen-tao, LIU Yong-fu, LI Rui-xin, DAI Ya-wen, CHENG Chun, TAN Peng, NI Meng. Rechargeable alkaline zinc batteries: Progress and challenges [J]. Energy Storage Materials, 2020, 31: 44−57. https://doi.org/10.1016/j.ensm.2020.05.028.

[36] YAN Chao-yi, WANG Xu, CUI Meng-qi, WANG Jiang-xin, KANG Wen-bin, FOO C Y, LEE P S. Stretchable silver−zinc batteries based on embedded nanowire elastic conductors [J]. Advanced Energy Materials, 2014, 4(5): 1301396. https://doi.org/10.1002/aenm.201301396.

[37] PAN Jun-qing, SUN Yan-zhi, WANG Zi-hao, WAN Ping-yu, LIU Xiao-guang, FAN Mao-hong. Nano silver oxide (AgO) as a super high charge/discharge rate cathode material for rechargeable alkaline batteries [J]. Journal of Materials Chemistry, 2007, 17(45): 4820−4825. https://doi.org/10.1039/b711373k.

[38] BERCHMANS S, BANDODKAR A J, JIA Wen-zhao, RAMÍREZ J, MENG Y S, WANG J. An epidermal alkaline rechargeable Ag−Zn printable tattoo battery for wearable electronics [J]. Journal of Materials Chemistry A, 2014, 2(38): 15788−15795. https://doi.org/10.1039/c4ta 03256j.

[39] YIN Qi-sheng, CHEN Li-bao, CHEN Yue-jiao, ZHAN Feng. A high-performance flexible aqueous silver−zinc rechargeable battery based on AgNP/CNT-graphite paper and ZnNF-graphite paper [J]. Composites Communications, 2021, 26: 100728. https://doi.org/110.22052/jns.2021.03.017.

[40] LEE J M, KIM J H, KIM S J. Fabricating a continuous fiber silver-zinc battery with micro-sized diameter [J]. ChemElectroChem, 2018, 5(22): 3361−3367. https://doi.org/10.1002/ celc.201801005.

[41] TAN Peng, CHEN Bin, XU Hao-ran, CAI Wei-zi, HE Wei, ZHANG Hou-cheng, LIU Mei-lin, SHAO Zong-ping, NI

Meng. Integration of Zn−Ag and Zn−air batteries: A hybrid battery with the advantages of both [J]. ACS Applied Materials & Interfaces, 2018, 10(43): 36873−36881. https://doi.org/10.1021/acsami.8b10778.

[42] WANG Jia-xin, LI Guang-she, LIU Xiao-qing, OUYANG Quan, MA Ming-wei, WANG Qiao, ZHANG Xin, FAN Zhi-peng, LI Li-ping. In-situ electrochemical oxidization of V_2O_3−C cathode for boosted zinc−ion storage performance [J]. Applied Surface Science, 2023, 616: 156481. https://doi.org/10.1016/j.apsusc.2023.156481.

[43] WANG Meng-lian, NIE Kai-qi, WU Hai-bo, LV Xiao-xin, DENG Jiu-jun, JI Hong-bing. Carbon nanotubes intertwined porous vanadium oxide heterostructured microfibers as high-performance cathodes for aqueous zinc-ion batteries [J]. Applied Surface Science, 2023, 612: 155791. https://doi.org/10.1016/j.apsusc.2022.155791.

黏结剂对水系 AgO−Al 电池正极材料电化学性能的影响

贺雪花[1]，王升贵[1,2]，王元奎[2]，徐万里[3]，宋觉敏[4,5]，李 政[4,5]，
张海涛[1]，杨光宙[1]，汪心怡[1]，张 倩[1]，李宏煦[6]，余 琨[1,5]

1. 中南大学 材料科学与工程学院，长沙 410083；
2. 中国船舶集团公司 第 705 研究所昆明分部，昆明 650032；
3. 军事科学院 系统工程研究所，北京 102300；
4. 湖南汇动新材料有限公司，湘潭 411101；
5. 湖南省中大特冶新材料研究院，长沙 410012；
6. 紫金矿业集团股份有限公司，厦门 361008

摘 要：为了改善水系过氧化银−铝(AgO−Al)电池正极材料动力学缓慢和机械强度较差的问题，研究不同黏结剂聚四氟乙烯(PTFE)和聚乙烯吡咯烷酮(PVP)对 AgO 正极材料的影响。通过扫描电子显微镜(SEM)、透射电子显微镜(TEM)、循环伏安法(CV)、交流阻抗谱(EIS)和恒电流放电测试对样品进行表征。结果表明，与纯 AgO 和 AgO−PTFE 电极相比，PVP 能有效地将电极材料结合在一起。制备的 AgO−PVP 作为 AgO−Al 电池的正极材料可提高电池容量，表现出高比容量(500 mA/cm^2 时为 389.95 mA·h/g)、高工作电压(500 mA/cm^2 时为 1.75 V)、最大能量密度(665.65 W·h/kg)和最大功率密度(5236 W/kg)。此外，还研究了 AgO−PVP 正极材料的电化学机理，发现该电极具有快速的离子扩散和有效的界面离子/电子传输能力。

关键词：AgO；正极材料；高比容量；黏结剂；水系 AgO−Al 电池

(Edited by Xiang-qun LI)